Jianguo Zhang
Yizhuo Li
Fengling Hu ✉
Peng Chen
Han Zhang
Liang Song
Youcheng Yu

https://doi.org/10.21278/TOF.483057523
ISSN 1333-1124
eISSN 1849-1391

HUMAN-ROBOT INTERACTION OF A CRANIOTOMY ROBOT BASED ON FUZZY MODEL REFERENCE LEARNING CONTROL

Summary

In this paper, we design a variable admittance controller and propose a variable admittance human-robot cooperative control method based on fuzzy model reference learning. The method is intended to improve the flexible adaptive capability of the robot to assist the surgeon in accomplishing different stages of the task during a craniotomy. First, the method establishes the autoregressive integrated moving average-Kalman filtering-blood pressure (ARIMA-Kalman-BP) model for the drag force prediction by taking the features of natural human arm motion as the reference model of fuzzy learning control, which solves the problem of the features of natural human arm motion being difficult to model. Then the tuning parameter rules for variable virtual damping and virtual mass of the fuzzy conductivity controller are trained by the learning mechanism. Subsequently, the variable conductivity control method based on the tuning of virtual damping and virtual mass parameters is developed by using the robot acceleration and the robot velocity as inputs, and the robot desired velocity and desired acceleration as outputs. The experimental results show that the method can meet the requirement of flexibility; the maximum error of human-machine cooperative velocity is 0.0014 m/s, and the maximum error of human-machine cooperative acceleration is lower than 0.0021 m/s^2. Compared with the fuzzy control based on the variable admittance parameter alone, this method has better tracking velocity and acceleration.

Key words: *craniotomy robot, movement intention, variable admittance control, fuzzy control, reference learning control*

1. Introduction

Craniocerebral trauma, as a neurosurgical system disease with an injury rate second only to extremity injury, has an in-hospital mortality rate of 7% to 12% [1]. Cranial openings are one of the most effective treatments for cranial lesions. However, because of the large number of central nerves and arterial vessels inside the skull, the surgeon needs to avoid these "dangerous" tissue structures to remove the bone flap, which requires a high level of surgical skill [1].

Moreover, during craniotomy, the surgeon needs to work with heavy cranial drills and milling tools for long periods of time. Surgeon's fatigue can increase the risk of surgery [2]. Patients cannot receive timely and effective treatment in primary hospitals because of their limited medical level and surgeons' qualifications. Robots and surgeons working together provide a feasible solution to the above problems.

Currently, surgical robots are primarily categorized into passive robots, master-slave operation robots, and human-machine collaborative robots [3]. Among them, the human-machine collaborative robot allows the surgeon to hold the end effector of the robotic arm and perform the surgery along the designated path, as shown in Figure 1. During the surgical procedure, the human-machine collaborative robot not only alleviates the physical strain on the surgeon but also maintains the surgeon's decision-making role. Therefore, considering the practical outcomes, the human-machine collaborative robot is more suitable for current craniotomy procedures. It offers improved operational efficacy and can be effectively utilized in craniotomies.

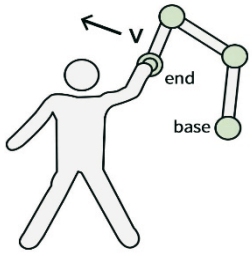

Fig. 1 Human-machine collaborative robot

In previous studies on human-robot interaction, admittance controllers have commonly been utilized to describe the relationship between external forces and the motion state of a robotic arm. However, traditional admittance controllers with fixed control parameters have inherent limitations. In human-robot collaborative tasks, these controllers often lack the flexibility to adapt to changes in human operator intentions and task requirements. For instance, consider a scenario where a human operator initiates the robot's motion, guides it to a target location, and eventually brings it to a stop. During these three stages, the robot needs to adjust its behaviour accordingly. Initially, when the human operator intends to start the motion, the robot should minimize energy dissipation from external forces exerted by the human and maximize acceleration. As the robotic arm gradually approaches the target location, it is essential to increase energy dissipation from external forces, minimize errors caused by human tremors, and enhance the precision of the robotic arm's motion. Additionally, due to the complex tissue structure of the brain and the small window area during surgery, there is a high demand for precision and force control when surgeons use robotic tools for milling along the surgical path. Traditional admittance control cannot reduce human errors and provide adequate safety guarantees for patients. Therefore, in this paper, we conduct in-depth research on the design of a variable impedance controller for the robot.

In the literature, one can find studies on human-computer interaction controllers based on human intentions. Among them, the majority use variable admittance controllers to realize the function of human-robot interaction. For example, Sirintuna et al. [4] realized adaptive control of robot position, velocity, and damping values by building a function-based rule model, thus ensuring that the admittance controller maintained a steady state during drilling tasks. In the studies by Ikeura et al. [5] and Li et al. [6], the virtual damping in the admittance control system is adjusted according to the velocity of the robotic arm. If the magnitude of the object's velocity is above or below the threshold, the person is assumed to accelerate or decelerate, respectively. Therefore, the guider damping is set to a low or a high value to promote or damp motion, respectively. On this basis, Aydin et al. [7] designed a fuzzy intention estimator to achieve smoother velocity transitions for robots. Lin et al. [8] and Hamad et al. [9] incorporated the natural characteristics of human motion as a reference model on top of the fuzzy controller, bringing the robot's motion closer to

the natural motion of the human arm. Guler et al. [10] proposed an artificial neural network-based variable admittance controller that adapts robot velocity in different task stages. Madan et al. [11] employed a support vector machine (SVM) classifier to train interactive strategies adaptable to multiple task modes based on human velocity and force signals.

The research conducted in the studies [4-11] primarily relied on the magnitude of simple force signals to determine human operations intent. In some studies, the force signals were processed in more depth in order to accurately characterize the change in force. For example, Duchaine et al. [12] and Tsumugiwa et al. [13] used the derivatives of velocity and interaction force to estimate the intended state of a human as acceleration or deceleration, and then adjusted the conductor damping accordingly. Rahman et al. [14] and Wang et al. [15] studied the adaptation of human arm stiffness based on force signals by implementing adaptive adjustments between stiffness and virtual damping to accommodate different stages of tasks.

All of the above studies used six-dimensional force sensors for the acquisition of external forces. In contrast, in the studies [16-18], the human body's electromyography signals are used to determine the human body's operations intent. However, using EMG signals for predicting human intentions has a significant drawback as it requires additional equipment attached to human limbs, limiting its practicality for physical human-robot interaction tasks in manufacturing environments. In contrast, Liu et al. [19] used a camera and motion capture system to train a deep learning-based human-computer interaction controller based on body movements. This requires a high number of images as well as computational efficiency.

Most of the variable-conductance controllers in the above literature are designed using end-of-arm velocity to describe the state of the robotic arm motion. However, in the context of surgical procedures, it is important to take into account that the end velocity of the robotic arm directly impacts both the surgical time and the surgeon's tactile feedback. Conversely, changes in the forces applied by the surgeon are directly manifested in the acceleration of the robotic arm's end. For example, when the rate of force change is less than zero, it implies a reduction in the arm's acceleration rather than a decrease in velocity [20], [21]. Therefore, in addition to the previous research [5-13], it is crucial to incorporate the consideration of acceleration into the analysis. Furthermore, while the magnitude of virtual damping directly influences the responsiveness of the robotic arm's end motion to changes in the applied forces by the surgeon, solely the adjustment of the virtual damping coefficient may compromise the overall stability of the system during complex tasks [20], [21]. Hence, it is necessary to supplement the existing literature [5, 8, 14, 15] with the exploration of virtual mass adjustments.

To address the aforementioned two issues, we propose the following control scheme:

Firstly, we propose estimating the surgeon's operations intent using the current end effector velocity and the computed acceleration from the previous time step under a compliance control model. Fuzzy control rules are established to relate these variables with the virtual mass and virtual damping in the compliance model. Secondly, the natural motion characteristics of the human arm are used as a reference model, and the fuzzy control rules are continuously adjusted through learning. To address the challenge of determining the start and end positions of variable-velocity arm motion in actual surgical procedures, an ARIMA-Kalman-BP model for predicting external forces exerted on the human body is developed. Finally, a variable admittance controller based on fuzzy control reference learning is designed. The inputs to the controller are the current end effector velocity and the computed acceleration, while the outputs are the desired end effector velocity and the desired acceleration. That is, this study realizes that the end velocity and acceleration of the robotic arm constantly approach the natural motion characteristics of the human arm in order to improve the suppleness and performance of the robot when assisting surgeons in surgery.

Compared with control schemes that only consider the velocity of the robotic arm, this approach ensures the continuity and smoothness of the arm's velocity profile, thereby enhancing the arm's

flexibility in responding to changes in external forces. The establishment of a reference model helps overcome the limitations of traditional fuzzy control which relies on subjective experience. Furthermore, compared with the variable-conductance control scheme, which only adjusts the virtual damping, this scheme supplements the consideration of the virtual mass and increases the stability performance of the system. Moreover, due to the influence of habits and the universality of human motion states, it is reasonable to establish an ARIMA-Kalman-BP model for predicting external forces exerted on the human body during drilling and grinding processes in craniotomies. This prediction is beneficial in addressing the issue of the force signals captured by force sensors lagging behind the surgeon's motion intention.

2. Design of variable admittance controller based on fuzzy model reference learning control (FMRLC)

With the research proposed in this paper, the collaboration between the robot and the surgeon is set up as shown in Figure 1. In order to detail the different control measures at each stage of the surgical process, only one-dimensional cooperative tasks are considered. The design scheme of the variable admittance controller based on the fuzzy model reference learning controller is shown in Figure 2.

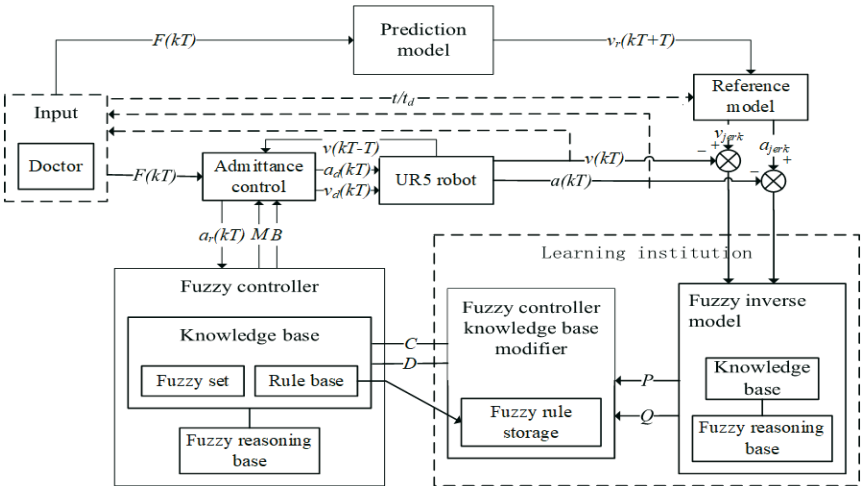

Fig. 2 Variable conductance control scheme based on fuzzy control reference learning control

As shown in Figure 2, the variable conductance control scheme based on fuzzy control reference learning control designed in this paper consists of a UR5 robot, a conductance controller, a fuzzy controller, a learning mechanism (fuzzy inverse model, fuzzy controller knowledge base modifier), a reference model, and a prediction model. Firstly, the surgeon's operations intent is inferred from the current motion velocity $v(kT\text{-}T)$ at the end of the robotic arm and the acceleration $a_r(kT)$ calculated for the previous moment in the conductance control model; these two are used as the inputs into the variable conductance fuzzy controller. Then the minimum plus acceleration model is introduced as the evaluation criterion of the motion state of the robotic arm; the aim is to determine how close it is to the natural motion state of the human arm. According to the difference between the velocity $v(kT)$ and the calculated acceleration $a_r(kT)$ at the end of the robotic arm and the velocity v_{jerk} and acceleration a_{jerk} in this model, the fuzzy control rules of virtual damping and virtual mass are adjusted by the learning mechanism to realize the adaptive variable conductance control. The equations of motion conforming to the minimum plus acceleration model are derived in this paper by establishing a prediction model to infer the velocity at the next moment, with the purpose of addressing the problem of accurate estimation of the termination time and termination position of the minimum plus acceleration model in practical applications. Finally, a fuzzy controller based on variable derivative rule adjustment is established with the input of the current motion

velocity $v(kT\text{-}T)$ at the end of the robotic arm and the calculated acceleration $a_r(kT)$ of the derivative model at the previous moment, and the output of the expected velocity $v_d(kT)$ and the expected acceleration $a_d(kT)$ at the end of the robotic arm.

The generic model of the conductive controller is:

$$F = Ma + Bv + Kx\,, \tag{1}$$

where K is the stiffness coefficient, and x is the actual displacement at the end of the robotic arm. Since the robot is not required to have a recovery force during the surgeon's dragging of the robot for surgery, K is made to be 0 [21]. Therefore, the conductance control model used in this paper is:

$$F = Ma + Bv \tag{2}$$

The control elements of the conductance controller are set as follows:

(1) The calculated acceleration at the current velocity of the robot's motion is obtained by using the derivative model of the previous moment, as shown in Equation (3):

$$a_r(k) = M(kT-T)^{-1}[F(kT) - B(kT-T)v(kT-T)]\,, \tag{3}$$

where $v(kT\text{-}T)$ is the current running velocity at the end of the robotic arm. The symbols $M(kT\text{-}T)$ and $B(kT\text{-}T)$ denote the values of virtual damping B and virtual mass M taken from the fuzzy model-based reference learning controller at the previous moment with the inputs $a_r(kT\text{-}T)$ and $v(kT\text{-}2T)$.

(2) The expected acceleration generated by the external force applied by the surgeon after the adjustment of the fuzzy model-based reference learning controller, with the robot moving at the current velocity, is shown in Equation (4):

$$a_d(kT) = M(kT)^{-1}[F(kT) - B(kT)v(kT-T)] \tag{4}$$

The expected velocity of motion of the robot is shown in Equation (5):

$$v_d(kT) = M(kT)^{-1}[F(kT) - B(kT)v(kT-T)]\cdot T + v(kT-T)\,, \tag{5}$$

where T is the sampling time, and $B(kT)$ and $M(kT)$ are adjusted for virtual damping and virtual mass by the fuzzy model-based reference learning controller with inputs $a_r(kT)$ and $v(kT\text{-}T)$.

2.1 Design of fuzzy controller

In the human-computer cooperation scenario discussed above, there are four types of movement intentions for the surgeon during craniotomy: uniform velocity, acceleration, deceleration, or stopping to reverse acceleration:

1) When the surgeon's motion intention is uniform velocity, the virtual damping and virtual mass are unchanged.

2) When the surgeon's motion intention is acceleration, the calculated acceleration is in the same direction as the current end velocity of the robotic arm; at this time, the virtual damping and virtual mass should be reduced according to the magnitude of acceleration.

3) When the surgeon's motion intention is to decelerate or stop, the calculated acceleration is reversed from the current velocity at the end of the robotic arm, at which time the virtual damping should increase and the virtual inertia decrease.

4) When the surgeon's motion intention is reversed, there are two stages: deceleration in the original direction until the velocity is 0, and then reverse acceleration. When decelerating, the virtual damping is increased. When accelerating in the reverse direction, the virtual damping is decreased.

Table 1 Initial rule table for fuzzy control of *B*

B / *v* \ a_r	-3	-2	-1	0	1	2	3
3	1	2	3	4	5	6	7
2	1	2	3	4	5	5	6
-1	3	3	3	6	6	5	5
0	4	5	6	7	6	5	4
1	5	5	6	6	3	3	3
2	6	5	5	4	3	2	1
3	7	6	5	4	3	2	1

Table 2 Initial rule table for fuzzy control of *M*

M / *v* \ a_r	-3	-2	-1	0	1	2	3
-1	1	2	3	7	5	2	4
-2	2	2	3	7	5	6	4
-3	3	3	3	6	5	5	4
0	5	5	6	6	6	5	5
1	5	5	5	6	3	2	2
2	6	6	5	7	2	2	2
3	4	4	4	7	2	2	1

Based on the above discussion, the fuzzy control uses a two-input, two-output (MIMO) model. The input of the fuzzy controller is set as the current end velocity of the robotic arm $v(kT\text{-}T)$ and calculated acceleration a_r $(kT)$of the robotic arm motion. The output of the fuzzy controller is set as $B(kT)$ and $M(kT)$. The inference rules can be set as follows:

If $\tilde{a}_{r1}$ is A_1^j and ... $\tilde{a}_{rs}$ is A_s^j , and $\tilde{v}_1$ is D_1^l and ... $\tilde{v}_s$ is D_s^k , then $\tilde{B}_n$ is $E_n^{j,...,k,l,...,m}$, $\tilde{M}_n$ is $C_n^{j,...,k,l,...,m}$, where $\tilde{a}_{rh}$, $\tilde{v}_h$, $\tilde{B}_n$ and $\tilde{M}_n$ (h=1,2,...,s) are the language variables related to the controller inputs v, a_r, and outputs B and M; A_s^i , D_s^i are the i-th language values of $\tilde{a}_{rs}$ and $\tilde{v}_s$, respectively; $E_n^{j,...,k,l,...,m}$ are the language values of $\tilde{B}_n$; and $C_n^{j,...,k,l,...,m}$ are the language values of $\tilde{M}_n$.

The theoretical domains [v_{min}, v_{max}] and [a_{rmin}, a_{rmax}] of the current velocity $v(k\text{-}1)$ and the calculated acceleration $a_r(k)$ at the end of the robotic arm are divided into 4 classes, which are subdivided into 7 fuzzy sets: $\tilde{v}_b = \{-3,-2,-1,0,1,2,3\}$ $\tilde{a}_{rb} = \{-3,-2,-1,0,1,2,3\}$. The theoretical domains [B_{min}, B_{max}] and [M_{min}, M_{max}] of the virtual damping coefficient B and virtual mass coefficient M are divided into 7 classes, which are subdivided into 7 fuzzy sets: $\tilde{B}_n = \{1,2,3,4,5,6,7\}$ $\tilde{M}_n = \{1,2,3,4,5,6,7\}$. The initial fuzzy control rules of B and M are shown in Table 1 and Table 2, respectively.

2.2 Reference mechanism design based on minimum acceleration model

Neville Hogan established the minimum jerk acceleration model to describe the natural motion process of the human arm. This model is commonly used internationally to evaluate the suppleness of the motion process [23]. Therefore, the process of arm movement during the surgeon's journey from the beginning to the end of the surgical path without the assistance of a robotic arm can be considered to conform to the minimum jerk acceleration model [24]. The minimum plus-plus acceleration model is shown in Equation (6):

$$x(t) = x_i + (x_f - x_i)\left(\left(\frac{10t}{t_d}\right)^3 - \left(\frac{15t}{t_d}\right)^4 + \left(\frac{16t}{t_d}\right)^5\right), \tag{6}$$

where x_i is the starting position, x_f is the end position, t/t_d is the normalized time, $x(t)$ is the motion displacement, t is the motion time, and t_d is the termination time.

In the process of craniotomy, the motion process of the surgeon dragging the robotic arm can be approximated to the human arm motion process, so as to improve the suppleness of human-computer interaction. Therefore, the reference model of the end velocity and acceleration of the robotic arm is set as follows:

$$v_{jerk} = \frac{\mathrm{d}x(t)}{\mathrm{d}t} \tag{7}$$

$$a_{jerk} = \frac{\mathrm{d}^2x(t)}{\mathrm{d}t^2} = \frac{\mathrm{d}v_{jerk}}{\mathrm{d}t}. \tag{8}$$

In this paper, v_{jerk} and a_{jerk} are defined as the ideal velocity and acceleration of the end motion of the robotic arm. According to Equations (6-8), there are two problems with the minimum additive acceleration model when applying it to robot-assisted surgery. The first is that this model is suitable for variable velocity motion. Therefore, it is not suitable when the surgeon keeps the end of the robotic arm moving at a uniform velocity. Consequently, in this paper, only the minimum acceleration model is applied to variable velocity motion. The ideal velocity v_{jerk} for uniform motion is defined as the initial velocity of the end of the arm at the time of uniform motion. Finally, we split the entire surgical path into a uniform motion segment and a variable velocity motion segment. The second problem is that the minimum acceleration model is related to the start and end positions and termination time. However, during the actual craniotomy, we cannot precisely determine the duration of the variable velocity motion and the beginning and end positions that the surgeon wants. To address this issue, we first calculate the motion equations of the robotic arm equivalent to the minimum jerk acceleration model based on Equations (6-8), as shown in Equation (9). Then, we establish a predictive model for the surgeon's dragging force and determine the surgeon's intended motion for the next stage based on Equations (2-4):

$$\begin{cases} x_{jerk}(t) = u_0 + u_1 t + u_2 t^2 + u_3 t^3 + u_4 t^4 + u_5 t^5 \\ v_{jerk}(t) = u_1 + 2u_2 t + 3u_3 t + 4u_4 t^3 + 5u_5 t^4 \\ a_{jerk}(t) = 2u_2 + 6u_3 t + 12u_4 t^2 + 20u_5 t^3 \end{cases}, \tag{9}$$

where u_i (i=0,1,2,3,4,5) is the time coefficient.

2.2.1 Prediction of surgeon’s intent based on the ARIMA-Kalman-BP model

The sensor picks up a lot of noise in the surgeon's operating force signal during the procedure. In this paper, the Kalman filter model can reduce the interference of noise in the force signal, and the state and measurement equations of the Kalman filter are shown in Equations (10, 11) [25], [26]:

$$F(kT) = \mathbf{\Phi} F(kT - T) + \mathbf{\Gamma} w(kT - T) \tag{10}$$

$$Z(kT) = \mathbf{H} F(kT) + \mu(kT)\ , \tag{11}$$

where $F(kT)$ is the state vector of the surgeon's operating force, $w(kT\text{-}T)$ is the state noise vector, $Z(kT)$ is the surgeon's operating force observation vector, $\mu(kT)$ is the observation noise vector, $\mathbf{\Phi}$ is the state transfer matrix, $\mathbf{\Gamma}$ is the excitation transfer moment, and $\mathbf{H}$ is the predicted output transfer matrix. According to Equations (9, 10), it is known that there are a large number of empirical-based settings for the establishment of their state and measurement equations.

To solve this problem, we establish ARIMA-based state equations and BP neural network-based measurement equations.

(1) ARIMA-based state equation

Establishing the linear state equation is the key to the Kalman filter algorithm model. Since the operating force signal captured during surgery is a time series and the magnitude of the surgeon's drag force at the current moment is influenced by the previous drag force state, the surgeon's drag force signal is regular. Therefore, we use the ARIMA (*p,d,q*) model. The *ar* model is an autoregressive model, the *ma* model is a sliding average model, and *d* is a force signal that requires d-order difference processing to obtain a smooth time series. The expressions of the ARIMA (*p,d,q*) model [27] are shown in Equations (12-15)：

$$F_t = c + \sum_{i=1}^{p} \gamma_i F_{t-i} + \sum_{i=1}^{q} \theta_i \varepsilon_{t-i} + \varepsilon_t \tag{12}$$

$$\gamma(l)(1-l)^d F_t = \theta(l)\varepsilon_t \tag{13}$$

$$\theta(l) = 1 - \theta_1 l - \theta_2 l^2 - \ldots - \theta_q l^q \tag{14}$$

$$\gamma(l) = 1 - \gamma_1 l - \gamma_2 l^2 - \ldots - \gamma_p l^p, \tag{15}$$

where γ_i (i=1,2,...,p) are the *ar* model parameters, θ_i (i=1,2,...q) are the *ma* model parameters, ε_t, ε_{t-1} ,..., ε_{t-p} is the white noise series, c is a constant, and l is the backward-shifting operator.

(2) Observations on the building of the BP neural network

The BP neural network model consists of an input layer, a hidden layer, and an output layer, which is a neural network model with forward propagation of information and backward propagation of error. In this paper, we set the operating forces at the first *kT, kT-T, ..., kT-(p-1)T* moments as inputs and the surgeon's operating force at moment *t=kT+T* as the output, based on the ARIMA model developed above. Then we choose a BP structural model with the number of neurons in the output layer N=10. The computational flow of the BP neural network mode is as follows [28]:

First, the training samples are processed step by step through the input, implicit, and output layers to get the final actual output values. This is the forward propagation process. Then the error between the actual output value and the training sample output value is calculated. Subsequently, Then the error between the actual output value and the training sample output value is calculated. If the error does not meet the required condition, backward propagation is needed to adjust the weights through the output layer and the hidden layer. The above two stages are repeatedly performed so that the error between the actual output value and the training sample output value is minimized until the error meets the required condition, then the calculation is terminated.

The prediction model is used to predict $F(kT+T)$, and the velocity and acceleration at the next moment are calculated as shown below:

$$a(kT+T) = M(kT-T)[F(kT+T) - B(kT-T)v(kT)] \tag{16}$$

$$v(kT+T) = M(kT-T)^{-1} a(kT+T)\cdot T + v(kT) \tag{17}$$

According to the Equations (16) and (17), the velocity of the robotic arm from $v(kT\text{-}10T)$ to $v(kT+T)$ is fitted in the form of Equation (18) to obtain the ideal velocity of the robotic arm:

$$v_{jerk}(t) = b_1 + b_2 t + b_3 t^2 + b_4 t^3 + b_5 t^4 \tag{18}$$

The ideal velocity model is differentiated to finalize the ideal acceleration for $t=kT$:

$$a_{jerk}(t) = b_2 + 2b_3 t + 3b_4 t^2 + 4b_5 t^3 . \tag{19}$$

2.3 Design of learning institution

The deviation of the controlled object velocity v from the reference model is expressed as follows, [6]:

$$y_e(kT) = v_{jerk} - v. \tag{20}$$

The rate of deviation of the controlled object velocity v from the reference model is

$$y_c(kT) = \frac{(y_e(kT) - y_e(kT - T))}{T}. \tag{21}$$

It is defined that the input of the fuzzy inverse model is $y_e(kT)$ and $y_c(kT)$, and the output is $P(kT)$ and $Q(kT)$. The fuzzy inverse model knowledge base is expressed in terms of fuzzy rules as:

If y_{e1}^{j} is G_1^j and ... y_{es}^{k} is G_s^k , and y_{c1}^{l} is H_1^l and ... y_{cs}^{m} is H_s^m , then $P_n^{j,...,k,l,...,m}$ is $W_n^{j,...,k,l,...,m}$, and $Q_n^{j,...,k,l,...,m}$ is $N_n^{j,...,k,l,...,m}$, where y_{eb}^{j} and y_{cb}^{l} (b=1,... ,s) are the fuzzy linguistic variables of the deviation variable and the deviation rate variable of the controlled object, respectively; $P_n^{j,...,k,l,...,m}$ and $Q_n^{j,...,k,l,...,m}$ are the resultant linguistic variables of and corresponding rules, respectively; $W_n^{j,...,k,l,...,m}$ and $N_n^{j,...,k,l,...,m}$ are the linguistic values corresponding to $P_n^{j,...,k,l,...,m}$ and $Q_n^{j,...,k,l,...,m}$, respectively; and G_1^d and H_1^d are the d-th linguistic values of y_{e1}^{j} and y_{c1}^{l}.

The fuzzy control rules of the fuzzy inverse controller are as follows:

1. When $y_e = 0$, $y_c = 0$, then take $P = 0$, $Q = 0$.
2. When $y_e > 0$, $y_c > 0$, then take $P < 0$, $Q < 0$.
3. When $y_e < 0$, $y_c < 0$, then take $P > 0$, $Q < 0$.

Table 3 Initial rule table for fuzzy control of P

P (y_e / y_c)	-4	-3	-2	-1	0	1	2	3	4
-4	1	0.8	0.6	0.6	0.4	0.4	0.2	0.2	0
-3	0.8	0.6	0.6	0.4	0.4	0.2	0.2	0	-0.2
-2	0.6	0.6	0.4	0.4	0.2	0	0	-0.2	-0.2
-1	0.6	0.4	0.4	0.2	0.2	0	-0.2	-0.2	-0.4
0	0.4	0.4	0.2	0.2	0	-0.2	-0.2	-0.4	-0.4
1	0.4	0.2	0.2	0	-0.2	-0.4	-0.4	-0.4	-0.6
2	0.2	0.2	0	-0.2	-0.2	-0.4	-0.4	-0.6	-0.6
3	0.2	0	-0.2	-0.2	-0.4	-0.4	-0.6	-0.8	-0.8
4	0	-0.2	-0.2	-0.5	-0.4	-0.6	-0.6	-0.8	-1

Table 4 Initial rule table for fuzzy control of Q

Q (y_e / y_c)	-4	-3	-2	-1	0	1	2	3	4
-4	-1	-1	-0.8	-0.8	-0.6	-0.4	-0.2	-0.2	0
-3	-1	-0.8	-0.8	-0.6	-0.4	-0.4	-0.2	0	-0.2
-2	-0.8	-0.8	-0.6	-0.4	-0.4	-0.2	0	-0.2	-0.2
-1	-0.8	-0.6	-0.4	-0.4	-0.2	0	-0.2	-0.2	-0.4
0	-0.6	-0.4	-0.4	-0.2	0	-0.2	-0.2	-0.4	-0.4
1	-0.4	-0.4	-0.2	0	-0.2	-0.2	-0.2	-0.4	-0.6
2	-0.2	-0.2	0	-0.2	-0.2	-0.4	-0.4	-0.6	-0.8
3	-0.2	0	-0.2	-0.2	-0.4	-0.4	-0.6	-0.8	-1
4	0	-0.2	-0.2	-0.8	-0.4	-0.6	-0.8	-1	-1

The domains of $y_e(kT)$, $y_c(kT)$ are set to be [-4,4]; they are divided respectively into 9 fuzzy sets: y_e={-4,-3,-2,-1,0,1,2,3,4} and y_c={-4,-3,-2,-1,0,1,2,3,4}. The theoretical domain of $P(kT)$ is set to [-1,1] and it is divided into 11 fuzzy sets P={-1, -0.8, -0.6, -0.4, -0.2, 0, 0.2, 0.4, 0.6, 0.8, 1}. The theoretical domain of $Q(kT)$ is [-1,0], and it is divided into 6 fuzzy sets Q={-1, -0.8, -0.6, -0.4, -0.2, 0}. The control rules of the fuzzy inverse controllers P and Q are shown in Table 3and Table 4, respectively. According to the control rules in Table 3 and 4, B and M are modified as shown in Equations (22-23):

$$C(kT) = B(kT - T) + P(kT) \tag{22}$$

$$D(kT) = M(kT - T) + Q(kT), \tag{23}$$

where $C(kT)$ and $D(kT)$ are the modified values of B and M, respectively.

3. Experimental design and results

3.1 Designing the surgical pathway in craniotomy

A virtual simulation platform is established by Simulink to verify the theoretical feasibility of FMRLC-based variable conductance control. An UR5 robot is used in this experiment. To simulate an actual craniotomy, we employ two-dimensional CT images of the skull for three-dimensional reconstruction, as shown in Figure 3. Typically, the cubic dimension of a human head is approximately 152.4 mm in width, 203.2 mm in height, and 190.5 mm in depth from front to back. The skull model established in this paper measures 195.2 mm in height, 150.5 mm in width, and 188.4 mm in depth from front to back, which conforms to the actual dimensions of a skull.

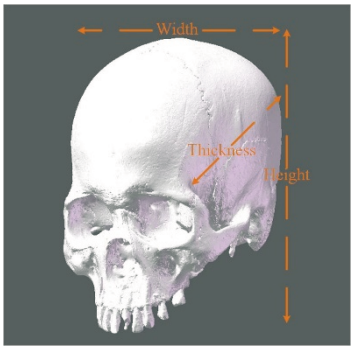

Fig. 3 Skull 3D reconstruction

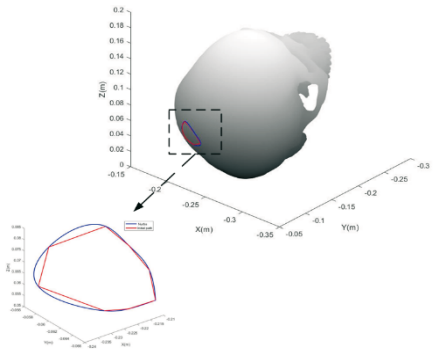

Fig. 4 Surgical path planning

The skull STL model is imported into MATLAB. Create a closed surgical path on the upper surface of the skull model using semi-automatic labelling:

1) Labelling of three borehole locations. (-0.21625, -0.0591183, 0.0813207), (-0.238889, -0.0578111, 0.0616928), (-0.21183, -0.652857, 0.057106).

2) Insert multiple labelled points between the drilled points to ensure that the area of the formed open window is larger than the tumour area.

3) Use the above labelled points as the starting points of the curve path by constantly searching for the nearest vertex from the previous vertex and connecting them, and then form a closed curve path.

4) In order to maintain the coherence of the path and ensure that the planned path is a smooth and feasible path, the non-uniform rational basis spline (NURBS) algorithm is used to smooth the path shown in Figure 4. The cranial model, the initial path and the path after smoothing using the NURBS algorithm are shown in Figures 3 and 4 respectively.

3.2 Experiments and analysis of the ARIMA-Kalman-BP model

To simulate the surgeon's intent to accelerate, decelerate, or stop the operation, the force signal is set as $F = -2\sin\left((\pi/4)t + 0.03\right)$. In order to simulate the noise of the force sensor, white noise with a noise power of 0.001 is added to this force signal. The overall experimental sampling time was 0.01 s, and the simulation time was 10 s. The force signal is shown in Fig. 5. The end of the UR5 robotic arm is set to move along the smoothed surgical path under the drag of this force signal.

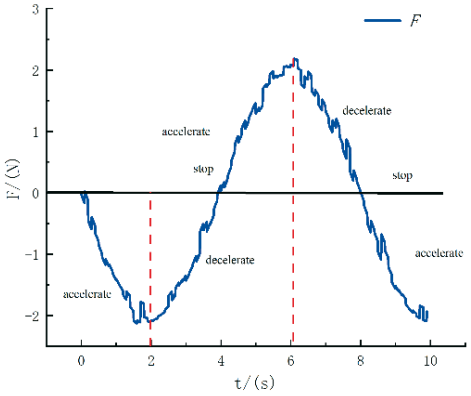

Fig. 5 Surgeon's operations intent and force signals

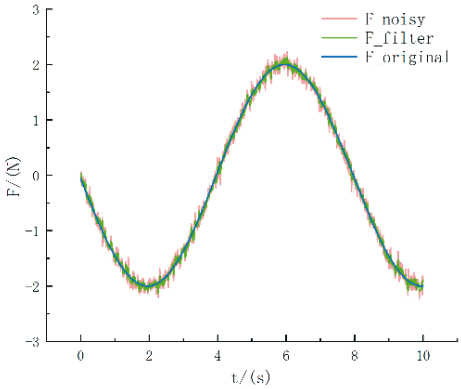

Fig. 6 Filtered force signals

(1) Data noise reduction processing

In order to avoid the interference of noise ion the experiment, the Kalman filter is used to reduce the noise of the force signal in this paper. Since this filter model is a single model, the observation output transfer matrix **H**, the state transfer matrix **Φ**, and the excitation transfer matrix **Γ** of this filter are set to 1. The final reduced-noise force signal, the force signal with added noise, and the original force signal are shown in Fig. 6.

In this paper, the first 70% of the filtered force is selected as the ARIMA-Kalman-BP model training sample, and the remaining 30% of the data is used as the ARIMA-Kalman-BP test sample data.

(2) Modelling of the ARIMA model

The training dataset is preprocessed using the second-order differencing method to achieve stationarity, and an ARIMA model is created. Based on the Akaike Information Criterion (AIC) [22] and the Bayesian Information Criterion (BIC), it is determined that the training dataset conforms to the ARIMA (6,0,5) model. The model coefficients are set as shown in Table 5.

Table 5 ARIMA (6,0,5) model coefficients

Autoregressive coefficient	φ_1	φ_2	φ_3	φ_4	φ_5	φ_6
	0.4809	1.1489	-0.0079	-0.3651	-0.2474	-0.0095
Moving average terms	θ_1	θ_2	θ_3	θ_4	θ_5	Constant term
	-0.03960	-1.0956	-0.0492	0.3252	0.2278	0.0023

(3) Modelling of the BP neural network model

Based on the ARIMA (6,0,5) model established above, we set the inputs of the BP neural network to be the data at moments kT-5T, kT-4T,…,T and the output to be the data at moment kT+T. Therefore, the training dataset for the model will consist of an input dataset of size 697x6 and a target output dataset (prediction dataset) of size 697x1. The number of neurons in the hidden layer is set to 10.

The remaining 30% of the force signal data was selected for validation in this study. The predicted results of the force signal are shown in Fig. 7. The errors in the predicted values of the ARIMA-Kalman-BP drag force prediction model with respect to the actual force signals are shown in Fig. 8. In Figs. 7 and 8, one can see that the prediction model results are close to the test data, and the error range of this prediction model is between [-0.15 N, 0.25 N]. The overall prediction effect is good.

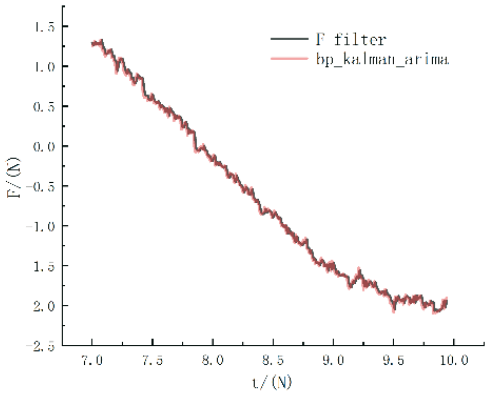

Fig. 7 Prediction of surgeon's intentions

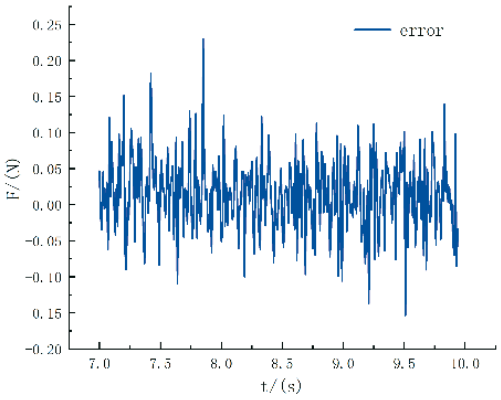

Fig. 8 The error range of the prediction model

3.3 Experiment using a variable admittance fuzzy control model based on FMRLC

In order to simplify the experiment, we only consider applying the above force signal in the x-axis direction at the end of the robotic arm. The initial virtual damping of the robotic arm along the top is preset to be 50 Ns/m and the initial virtual mass is 25 kg. The range of the operating force of the surgeon is set to be [-2.5 N, 2.5 N]. The range of velocity at the end of the robotic arm is [-0.01m/s, 0.01m/s]. The range of acceleration at the end of the robotic arm is [-0.01 m/s^2, 0.01 m/s^2]. The virtual damping coefficient range is [10 Ns/m, 220 Ns/m]. The range of the virtual mass coefficient is [5 kg, 185 kg]. The current velocity, calculated acceleration, virtual damping, and virtual mass are distributed equally in the corresponding fuzzy sets.

In this paper, the experimental group is set up as a variable admittance fuzzy control model based on FMRLC, and the comparison group is set up as a variable admittance fuzzy control model without FMRLC. The end effectors of the UR5 robotic arms in both the experimental and comparison groups perform back-and-forth movements under the drag of the force signal, as shown in Figures 9 and 10.

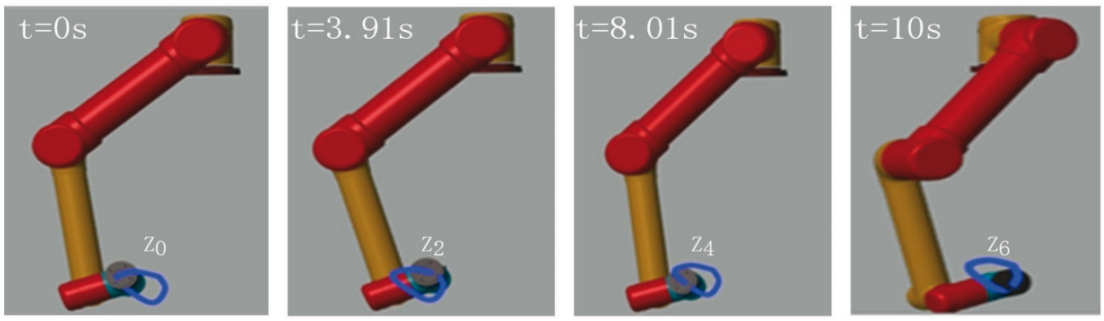

Fig. 9 The motion status of the robotic arm of the experimental group.

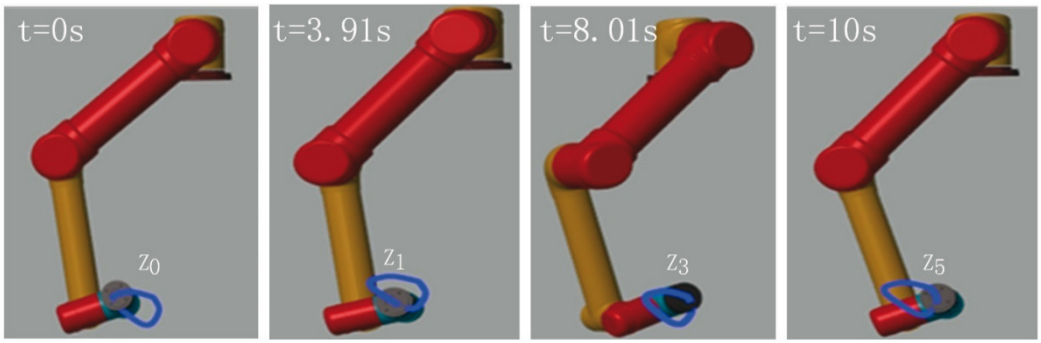

Fig. 10 The motion status of the robotic arm of the comparison group.

As shown in Figures 9 and 10, at the initial moment, the robotic arms are both at Z_0 (-0.2118, -0.655, 0.0571); at t = 3.91 s, the robotic arm of the comparison group arrives at the point Z_1 (-0.2391, -0.0575, 0.0625), whereas the robotic arm velocity of the experimental group are lower than those of the comparison group, arriving at the point Z_2 (-0.2390, -0.0575, 0.0625). At t = 8.01 s, the robotic arm of the comparison group moved to the point Z_3 (-0.2197, -0.0581, 0.0818); the robotic arm of the experimental group reached the point Z_4 (-0.2131, -0.0604, 0.0769). At t = 10 s, the robotic arm of the comparison group reaches the Z_5 (-0.2285, -0.0565, 0.0761) point, while the experimental group reaches the point Z_6 (-0.2267, -0.0567, 0.0776). From this, we can learn that in the period from 0 to 3.91 s, the average movement velocity of the robotic arm of the experimental group is not much different from the average movement velocity of the robotic arm of the comparison group; in the period from 3.92 s to 10 s, the average movement velocity of the robotic arm of the experimental group is higher than the average velocity of the robotic arm of the comparison group.

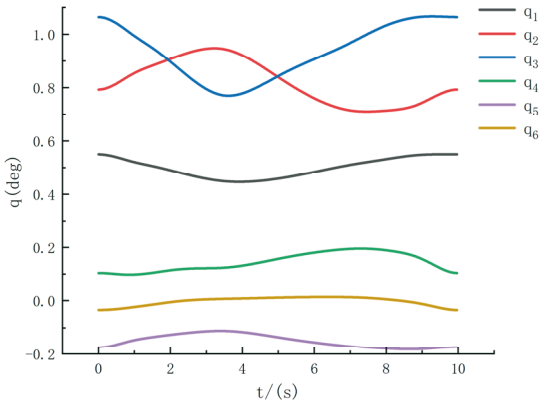

Fig. 11 The variation curves of joint angles.

Figure 11 shows the joint angle variation curves of the robotic arm in the variable admittance fuzzy control model based on FMRLC. The smooth variation of joint angles not only improves the precision of the robotic arm movements but also helps to reduce vibrations and instability during operation, thereby enhancing the overall performance. Therefore, the FMRLC-based variable admittance fuzzy control model provides an effective means for the motion control of robots, enabling the robotic arm to achieve smooth and precise movements, thereby offering higher-quality assistance for neurosurgical procedures.

In the following section, we will further analyse the changes in the velocity and acceleration of the robotic arm.

The control of the movement velocity of the robotic arm end in the experimental group and the comparison group is shown in Figs. 12 and 13. In the overall experimental process, the movement velocity of the robotic arm end in the experimental group is closer to the ideal movement velocity than that in the comparison group. Due to the smaller virtual damping and virtual mass settings under the initial fuzzy control rule, the motion velocity of the robotic arm in the experimental group v_1, a_1, and the comparison group v_0, a_0 is greater than the v_{jerk}, a_{jerk}. In addition, all of them exhibit a gradually increased gap between the obtained values for velocity and acceleration and those of the ideal velocity and acceleration. Subsequently, with the adjustment of the fuzzy control rules, the experimental group velocity and acceleration gradually approach the ideal velocity and acceleration. The mean and maximum error values and Pearson's coefficients of the errors between the velocity and acceleration of the robotic arm end movement, and the ideal velocity and acceleration for the experimental group and the comparison group are shown in Tables 6 and 7.

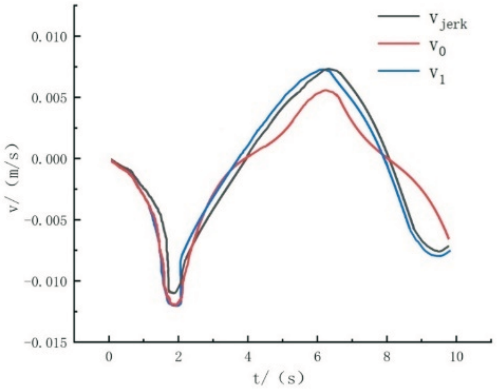

Fig. 12 Velocity curve

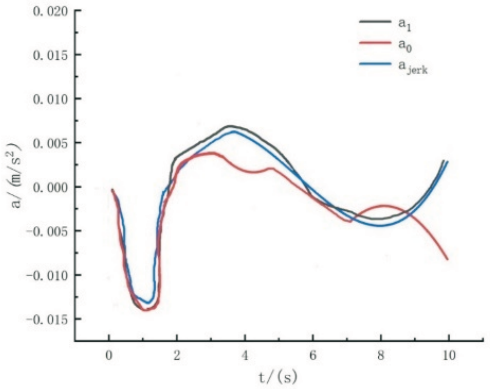

Fig. 13 Acceleration curve

Table 6 Velocity error mean and Pearson's coefficient

	Experimental group	Comparison group
Average error	0.0007 m/s	0.0013 m/s
Pearson's coefficient	0.9951	0.9530
Maximum error	0.0014 m/s	0.0040 m/s

Table 7 Acceleration error average and Pearson's coefficient

	Experimental group	Comparison group
Average error	0.0005 m/s^2	0.0033 m/s^2
Pearson's coefficient	0.9955	0.8891
Maximum error	0.0021m/s^2	0.0120m/s^2

In order to validate the effectiveness of our model, we will conduct a detailed comparison with other studies. Lin et al. [8] proposed a variable admittance human-robot cooperation control method based on fuzzy model reference learning. In comparison with our study, their method also uses the minimum jerk acceleration model as a reference model. However, the difference lies in the fact that the research conducted by Lin et al. only establishes fuzzy control rules for drag force, robotic arm velocity, and virtual damping. Lin and his collaborators did not consider the variation in robotic arm acceleration and virtual mass in the admittance controller. The results of the study done by Lin et al. are compared with the results of the current study, as shown in Table 8.

Table 8 Average error and maximum error

	Average error	Maximum error
Lin et al.	0.0054 m/s	0.017 m/s
This study	0.0007 m/s	0.0014 m/s

In the above table, one can see that, compared with the fuzzy controller design that only considers robotic arm velocity and virtual damping, the design scheme of the fuzzy controller that additionally considers acceleration and virtual damping is more efficient in achieving a closer alignment between the robotic arm motion state and the natural characteristics of human arm movement.

In the study by Guler et al. [10], a supervised learning approach based on an artificial neural network (ANN) model is proposed for real-time classification of subtasks in physical human-computer interaction (pHRI) tasks involving exposure to rigid environments. During the sub-task switching process, when the force signal curve rises smoothly from 0 N to 40 N in 5 s, the velocity of the robotic arm decreases rapidly from 20 mm/s to 0 mm/s in about 0.5 s, which does not lead to the stabilization of the robotic arm movement. In contrast, our research, as shown in Fig.12, results in a smooth velocity curve and stable motion status of the robotic arm, which is crucial for surgical safety considerations.

$$Y(s) = \frac{v(s)}{F(s)} = \frac{1}{ms^{\alpha} + b} \tag{24}$$

4. Conclusion

In order to fully satisfy the surgeon's intention to perform craniotomy, we propose a variable- admittance control scheme based on fuzzy model reference learning control. It is experimentally demonstrated that, compared with traditional fuzzy controllers, our scheme introduces a learning reference model and makes the motion state of the robotic arm closer to the natural state of the surgeon's arm by means of continuously adjusted fuzzy rules. Our research is applied to a scenario in which a surgeon drags a robotic arm to perform milling along a surgical path.

In the future, we aim to test our approach in simulated real surgical human-robot interaction scenarios to further validate its potential in craniotomy. To this end, we have established an experimental platform for a variable-conductance control scheme based on fuzzy model reference learning control. The experimental platform consists of a UR5 robotic arm, a SUI robotic FT300 six-dimensional force transducer, a test bench and a marker pen. First, we designed the path on the surface of the skull. The operator manually dragged the end of the robotic arm to move the marker along the pre-planned path. The entire motion process records the trajectory of the end point of the robotic tool through coordinate paper. The position and velocity information of the end of the surgical tool is obtained by reading the value of the encoder in real time.

We will also conduct in-depth research and make improvement based on the experimental results to improve the accuracy and softness of robot-assisted craniotomy.

Acknowledgments

This research was supported by the Science and Technology Commission of Shanghai Municipality, Science, Technology and Innovation Action Plan (grant number: 23141901400), Collaborative Innovation Fund of Shanghai Institute of Technology (grant number: XTCX2023−18), and Youth Foundation of Zhongshan Hospital, Fudan University (grant number:2022−005).

REFERENCES

[1] Sun, X.C. Study on Impedance Control of Craniotomy Robot, *Tianjin, China: Tianjin University of Technology.* 2021. https://doi.org/10.27360/d.cnki.gtlgy.2021.000607

[2] Cui, M.; Ma, X.D.; Zhang, M.; Zhu, W. Advances in neurosurgical craniotomy robotic research. *Journal of the People's Liberation Army Medical College*, 2019, 40(01):95-97+101.

[3] Tang, Y.C. "Research on human-machine cooperative control method for orthopedic surgery robot based on variable admittance", *Suzhou, China: Suzhou University.* 2019. https://doi.org/10.27351/d.cnki.gszhu.2019.000889

[4] Sirintuna, D. et al. (2020) 'A Variable-Fractional Order Admittance Controller for pHRI', 2020 IEEE International Conference on Robotics and Automation (ICRA), Robotics and Automation (ICRA), 2020 IEEE International Conference on, pp. 10162–10168. https://doi.org/10.1109/ICRA40945.2020.9197288

[5] Ikeura, R.; Moriguchi, T.; Mizutani, K. Optimal variable impedance control for a robot and its application to lifting an object with a human. In Proceedings. *11th IEEE International Workshop on Robot and Human Interactive Communication*, 2002:500-505.

[6] Li, J.Q; Qi, H.J; Zhang, G.P; Zhao, H. W; Guo, S.J. (2018) Human - robot coordination movement control method based on force information. Computer Integrated Manufacturing Systems,2018,24(08):2005-201

[7] Y. Aydin, N. Arghavani, and C. Basdogan, "A new control architecture for physical human-robot interaction based on haptic communication," in Proc. ACM/IEEE Int. Conf. Hum. -Robot Interaction, 2014, pp. 122–123. https://doi.org/10.1145/2559636.2563682

[8] Lin, A.D.; Gan, M. F.; Ge, H.; Tang, Y.C.; Xv, H.D. Kuang, S.L.,…, Sun, L.N., Human-robot interaction for surgical robots based on fuzzy model reference learning control. Robot. 2019,41(04):543-550. https://doi.org/10.13973/j.cnki.robot.180495

[9] Hamad, Y.M., Aydin, Y. and Basdogan, C. (2021) 'Adaptive Human Force Scaling via Admittance Control for Physical Human-Robot Interaction', IEEE Transactions on Haptics, Haptics, IEEE Transactions on, IEEE Trans. Haptics, 14(4), pp. 750–761. https://doi.org/10.1109/TOH.2021.3071626

[10] Guler, B. et al. (2022) 'An adaptive admittance controller for collaborative drilling with a robot based on subtask classification via deep learning', Mechatronics, 86. https://doi.org/10.1016/j.mechatronics.2022.102851

[11] Madan C E, Kucukyilmaz A, Sezgin TM, Basdogan C. Recognition of haptic interaction patterns in dyadic joint object manipulation. IEEE Trans Haptics 2014;8(1):54–66. https://doi.org/10.1109/TOH.2014.2384049

[12] Duchaine, V.; Gosselin, C. M. General model of human-robot cooperation using a novel velocity based variable impedance control. In Second Joint EuroHaptics Conference and Symposium on Haptic Interfaces for Virtual Environment and Teleoperator Systems (WHC'07). IEEE, 2007:446-451. https://doi.org/10.1109/WHC.2007.59

[13] Tsumugiwa, T.; Yokogawa, R.; Hara, K. Variable impedance control with regard to working process for man-machine cooperation-work system. In Proceedings 2001 IEEE/RSJ International Conference on Intelligent Robots and Systems. Expanding the Societal Role of Robotics in the the Next Millennium (Cat. No. 01CH37180). IEEE,2001: 3, 1564-1569.

[14] M. Rahman, R. Ikeura and K. Mizutani, "Investigating the impedance characteristics of human arm for development of robots to cooperate with human operators," in Proc. IEEE Int. Conf. Syst., Man, Cybern.,1999, pp. 676–681.

[15] Wang, F; Chao, Z.Q; Zhang C.Q; Li, H.Y. Variable Admittance Control Simulation of robot Based on Trajectory Tracking of Human Arm Motion. computer simulation, 2018,35(12):280-285.

[16] Anvaripour, M.; Khoshnam, M.; Menon, C.; Saif, M. Safe human robot cooperation in task performed on the shared load. 2019 International Conference on Robotics and Automation (ICRA). IEEE, 3761-3767. https://doi.org/10.1109/ICRA.2019.8794176

[17] Grafakos, S.; Dimeas, F.; Aspragathos, N. Variable admittance control in pHRI using EMG-based arm muscles co-activation. 2016 IEEE International Conference on Systems, Man, and Cybernetics (SMC). IEEE, 2016:001900-001905. https://doi.org/10.1109/SMC.2016.7844516

[18] Noughaby, A. G.; Vossoughi, G. R. The control of an exoskeleton and the reduction of interaction force using human intent detection by EMG signals and torque estimation. In 2018 6th RSI International Conference on Robotics and Mechatronics (ICROM). IEEE, 2018:536-541. https://doi.org/10.1109/ICRoM.2018.8657584

[19] Liu, S., Zhang, J., Zhang, Y. et al. A wearable motion capture device able to detect dynamic motion of human limbs. Nat Commun 11, 5615 (2020). https://doi.org/10.1038/s41467-020-19424-2

[20] Zhou, C.Z.; Ye, Z.; Xie, L. Human-computer interaction strategy for variable admittance control of robot based on force sensor. Journal of Jiangxi Normal University (Natural Science Edition), 2020,44(03):221-225+234. https://doi.org/10.16357/j.cnki.issn1000-5862.2020.03.01

[21] Lecours, A.; Mayer-St-Onge, B.; Gosselin, C. Variable admittance control of a four-degree-of-freedom intelligent assist device. In 2012 IEEE international conference on robotics and automation. IEEE, 2012:3903-3908. https://doi.org/10.1109/ICRA.2012.6224586

[22] Zhou, C.B. Research on robot load recognition and flexible control, Shenyang, China: Shenyang University of Technology. 2022. https://doi.org/10.27322/d.cnki.gsgyu.2022.000917

[23] Hogan, N. (1984), An organizing principle for a class of voluntary movements. Journal of neuroscience, 4(11), 2745-2754. https://doi.org/10.1523/JNEUROSCI.04-11-02745.1984

[24] Song, S.Q. Study on variable admittance control method of rope drive joint replacement robot. Harbin, China: Harbin Institute of Technology. https://doi.org/10.27061/d.cnki.ghgdu.2021.003937

[25] Wang, Z.X. (2004), Optimal state estimation and system identification. Xi'an, China: Northwestern Polytechnical University Press.

[26] Chen, H., He, J., Ma, K, Huang, Q., UWB fine location algorithm based on BP neural network compensated Kalman filter. Electronic design engineering, 2019,27(24):103-107. https://doi.org/10.14022/j.issn1674-6236.2019.24.023

[27] Xu, E.S.; Lu, W.H.; Liu, Y.F.; Li, B.L.; Li, Y. Research on Data Fusion Algorithm and Application based on Kalman Filter. Computer technology and development. 2020,30(05):143-147.

[28] Pan, D.F.; Liu, H.; Li, Y.F. A wind velocity forecasting optimization model for wind farms based on time series analysis and Kalman filter algorithm. Power grid technology. 2008(07):82-86.

Submitted: 26.8.2023

Accepted: 07.3.2024

Jianguo Zhang[1]
Yizhuo Li[1]
Fengling Hu*[2,3]
Peng Chen[1]
Han Zhang[1]
Liang Song[4]
Youcheng Yu[3]
[1]School of mechanical engineering,
Shanghai Institute of Technology,
No 100 Haiquan Rd, Shanghai, China
[2]Shanghai Geriatric Medical Center,
No 2560, Chunshen Rd, Shanghai, China
[3]Department of Stomatology, Zhongshan Hospital, Fudan University,
No 180 Fenglin Rd, Shanghai, China
[4]Department of Stomatology, Shanghai Fifth People's Hospital, Fudan University,
No 128, Ruili Rd, Shanghai, China
*Corresponding author:
flhu201418@163.com